



**HAL**  
open science

# Synchronized autonomous sampling reveals coupled pulses of biomass and export of morphologically different diatoms in the Southern Ocean

Stéphane Blain, Mathieu Rembauville, Olivier Crispi, Ingrid Obernosterer

► **To cite this version:**

Stéphane Blain, Mathieu Rembauville, Olivier Crispi, Ingrid Obernosterer. Synchronized autonomous sampling reveals coupled pulses of biomass and export of morphologically different diatoms in the Southern Ocean. *Limnology and Oceanography*, 2020. hal-03002231

**HAL Id: hal-03002231**

**<https://hal.science/hal-03002231>**

Submitted on 12 Nov 2020

**HAL** is a multi-disciplinary open access archive for the deposit and dissemination of scientific research documents, whether they are published or not. The documents may come from teaching and research institutions in France or abroad, or from public or private research centers.

L'archive ouverte pluridisciplinaire **HAL**, est destinée au dépôt et à la diffusion de documents scientifiques de niveau recherche, publiés ou non, émanant des établissements d'enseignement et de recherche français ou étrangers, des laboratoires publics ou privés.

1 Synchronized autonomous sampling reveals coupled pulses of biomass and export of  
2 morphologically different diatoms in the Southern Ocean

3

4 Stéphane Blain\*, Mathieu Rembauville, Olivier Crispi and Ingrid Obernosterer

5 Sorbonne Université, CNRS, Laboratoire d'océanographie microbienne, avenue Pierre Fabre,

6 66650 Banyuls sur mer, France

7

8 [stephane.blain@obs-banyuls.fr](mailto:stephane.blain@obs-banyuls.fr)

9 [mathieu.rembauville@obs-banyuls.fr](mailto:mathieu.rembauville@obs-banyuls.fr)

10 [olivier.crispi@obs-banyuls.fr](mailto:olivier.crispi@obs-banyuls.fr)

11 [ingrid.obernosterer@obs-banyuls.fr](mailto:ingrid.obernosterer@obs-banyuls.fr)

12

13 \* Corresponding author

14

15 keywords : carbon stock, carbon export, diatoms, southern ocean, aggregates, seasonal time

16 series, autonomous sampling

17 Running head : Pulses of diatom biomass and export

18

19

20 ABSTRACT.

21

22 The Southern Ocean hosts a large diversity of diatoms that play a major role in carbon fluxes.

23 How the seasonal dynamics in the abundance of specific taxa in surface waters are linked to

24 their contribution to carbon export remains, however, poorly understood. We present here

25 synchronized observations from autonomous samplers deployed in the mixed layer (42 m)

26 and at depth (300m) during an entire productive season (October 2016 to March 2017) in

27 the iron fertilized region of the central plateau of Kerguelen. Microscopic observations of

28 surface water collected every 11 days revealed 30 different diatom taxa, each contributing

29 to > 1% of total carbon biomass throughout the season. The synchronised sampling revealed

30 a common pattern for diatom taxa belonging to 12 different genera, consisting, for a given

31 taxon, in short pulses of abundance in surface waters followed by export. We explain these

32 coupled dynamics by the formation of aggregates that are produced when a critical diatom

33 cell abundance is reached. This control of the maximum abundance of a given diatom drives

34 the seasonal change in the slope of the size-class distribution of the diatom community. It

35 further constrains the total carbon diatom biomass in a narrow range of values due to the

36 inverse relationship between total diatom abundance and their community-weighted mean

37 biomass. This coupling let us conclude that aggregate formation, and the export to depth,

38 occurs throughout the season for diatoms with different morphologies.

39

40

## 41 Introduction

42 During the past 250 million years diatoms have evolved a large diversity of forms and life  
43 styles (Armbrust 2009). They are successful unicellular phototrophic organisms that are  
44 present in almost all aquatic environments. They are characterized by an ornamented  
45 siliceous cell wall with diverse forms that serve as morphological criteria for species  
46 classification, an approach that is today complemented by DNA sequencing (Malviya et al.  
47 2016). From a biogeochemical perspective, diatoms play a central role in the carbon cycle  
48 (Tréguer et al. 2018). In the past they have contributed to the lowering of atmospheric CO<sub>2</sub>  
49 thanks to their efficiency to massively bury carbon in the sediment (Katz et al. 2005) and  
50 thereby formed large reservoirs of fossil fuels. In the contemporary ocean they contribute to  
51 40 % of global primary production (Nelson et al. 1995) and they sustain marine food webs.  
52 The success of diatoms is attributed to several features. On the one side, genomic  
53 adaptations (Armbrust et al. 2004; Allen et al. 2011) allow diatoms to thrive in various  
54 environments. They form blooms that can result in large sinking fluxes but require  
55 substantial nutrient supply, as provided in well-mixed water columns. This occurs  
56 preferentially in regions where turbulent water columns dominate (Margalef 1978). On the  
57 other side, the siliceous armour provides an efficient protection against predators, and  
58 possibly also against parasites and pathogens (Hamm and Smetacek 2007). The dense  
59 frustule enhances cell sinking (Smetacek 1985), necessitating elaborated strategies for  
60 maintaining the cells in the euphotic zone during the growth period (Raven and Waite 2004).  
61 The Southern Ocean hosts abundant and diverse communities of diatoms. Their ecology has  
62 been extensively described thanks to expeditions in different regions of the Antarctic  
63 circumpolar current (Queguiner et al. 1997; Tremblay et al. 2002; Leblanc et al. 2005) and to  
64 observations realised in naturally iron fertilized regions (Korb et al. 2008; Salter et al. 2012;

65 Lasbleiz et al. 2016) or during artificial fertilization experiments (Gall et al. 2001; Assmy et al.  
66 2013). Additional information was also gathered from investigations on the sinking en masse  
67 of the giant diatoms like *Rhizosolenia* spp. and *Thalassiothrix* spp. (Kemp et al. 2006) or of  
68 empty cells of *Corethron criophylum* (now named *Corethron pennatum* (Grunow) Ostenfeld )  
69 after entering the sexual stages (Crawford et al. 1997). One of the main motivation to link  
70 diatom ecology and biogeochemistry lies in the critical role they play in the carbon cycle  
71 (Tréguer et al. 2018). Their role as vectors of carbon export in the water column and storage  
72 at the seafloor has been demonstrated using sediment traps (Salter et al. 2012; Rigual-  
73 Hernández et al. 2015; Rembauville et al. 2015a) and by the examination of sediments (Allen  
74 et al. 2005; Armand et al. 2008; Rigual-Hernández et al. 2016). Considering all these  
75 observations, conceptual frameworks linking diatom ecology and the carbon cycle in the  
76 Southern Ocean were derived.

77 Different biogeochemical roles were attributed to different diatom taxa (Quéguiner 2013;  
78 Assmy et al. 2013). For example, fast growing taxa characterized by en masse sinking  
79 behaviour (e.g. *Chaetoceros*, *Thalassiosira*) were described as carbon sinkers or type 1, and  
80 highly silicified slow growing species as silica sinkers or type 2. The dominance of one  
81 category over the other leads to a strong decoupling between the carbon and silicon cycles  
82 (Assmy et al. 2013). However, the coupling between the temporal dynamics of surface  
83 stocks and export at depth of diatoms at the taxon level is still poorly studied and  
84 understood, because it requires to collect samples evenly spaced in time during the entire  
85 growth season. This task is particularly challenging in the open ocean and even more in  
86 harsh environments like the Southern Ocean. In our study we have addressed this issue  
87 using synchronized autonomous samplers deployed for 4 months both within (42 m) and  
88 below (300 m) the surface mixed layer. Our samples were collected in the long lasting

89 Southern Ocean blooms that are sustained by natural iron fertilization above the Kerguelen  
90 Plateau (Blain et al. 2007). Throughout the season, these blooms are dominated by a  
91 succession of different diatom taxa (Lasbleiz et al. 2016; Rembauville et al. 2017). This  
92 contrasts with spring to summer transitions in most oceanic regions where a succession of  
93 diatoms and non diatoms are observed (Barber and Hiscock 2006). The Kerguelen plateau  
94 waters therefore represent a unique environment for our investigations.

95

96 MATERIALS AND METHODS

97 **Moorings.**

98 Two moorings were deployed during the SOCLIM cruise (doi/10.17600/16003300), one for  
99 the sediment traps on 13 October 2016, and one in subsurface waters on 18 October 2016.  
100 Both moorings were recovered on 7 April 2017. The sub surface mooring (50°37'135 S /  
101 072°06'179 E, bottom depth 527m) was equipped with an aluminium framework located at  
102 42 m below the surface that contained a remote access sampler (RAS Mac Lane) allowing the  
103 collection of 48 x 500 mL samples. We collected 12 samples of unfiltered seawater every 11th  
104 day, preserved either with glutaraldehyde or mercury chloride, and 18 filtered and unfiltered  
105 samples preserved with mercury chloride (Fig 1a). The sub surface framework was also  
106 equipped with a CTD sensor (SeabirdSBE 16) and a current meter (Aquadrop). Below the  
107 instrument package and down to 300 m, the mooring line was equipped with additional  
108 temperature (SBE 56) and temperature/salinity sensors (SBE 37) to monitor changes in the  
109 mixed layer depth. The second mooring (50°38'344 S/ 71°59'854E, bottom depth 527 m) was  
110 equipped with a Technicap PPS3 sediment trap (0.125 m<sup>2</sup> collecting area, 4.75 aspect ratio)  
111 located at 300 m below the surface. The 12 cups (250 ml) were filled with 5% formalin  
112 hypersaline solution buffered at pH=8 with sodium tetraborate. The collection time for each  
113 cup was 11 days. After recovery of the RAS mooring the samples were immediately  
114 transferred from the bag into 500 mL clean polycarbonate bottles and stored in the dark at  
115 room temperature until processing in the laboratory. For the sediment traps, 1 ml of the  
116 supernatant of the cups were replaced by fresh hypersaline formalin buffered (pH=8)  
117 solution before storage at room temperature. Upon recovery of the cups in the laboratory,  
118 the swimmers were removed and the samples split into eight aliquots using a Jencons  
119 peristaltic splitter (Rembauville et al. 2015b)

## 120 **Microscopy and morphometry**

121 Microscopic observations were conducted within four months after recovery of the  
122 moorings. For the identification of diatoms, counting and size measurements, we used the  
123 protocol described by (Salter et al. 2012) and modified by Rembauville et al. 2015a that  
124 allows to separately consider full and empty cells. This issue is critical for our work which  
125 aims to reconstruct the carbon flux and stock attributed to diatoms. For the preparations of  
126 diatom counting (RAS or TRAP) the samples were processed as follows. For the RAS,  
127 depending on the diatom abundance, 20 mL, or 2 mL diluted with 18 mL of artificial  
128 seawater (S=34), were decanted in a Sedgewick Rafter counting chamber (Pyser SGE S52,  
129 1mL chamber volume). For the trap samples, 2mL of one-eighth aliquot was diluted with 18  
130 mL of artificial seawater and decanted in a Sedgewick Rafter counting chamber. Diatoms  
131 were enumerated and identified under an inverted microscope with phase contrast  
132 (Olympus IX170) at magnification 400X. The morphometric measurements were done using  
133 high resolution images (Olympus DP71 camera) and Fiji image processing software. The  
134 biovolume was calculated from morphometric measurements (Hillebrand et al. 1999). The  
135 carbon content was derived from biovolumes using allometric relationships reported in the  
136 literature (Menden-Deuer and Lessard 2000; Cornet-Barthau et al. 2007) and taking into  
137 account specific relationships for spores (Rembauville et al. 2015a). The size-abundance  
138 distributions of the diatom community collected at a given time point was based on an  
139 octave (log<sub>2</sub>) scale of cell volume.

## 140 **Diatom carbon stocks and export fluxes.**

141 The carbon stock accounted for by diatoms was calculated by summing up the contributions  
142 of the different taxa. The integrated diatom carbon stock was calculated by multiplying the



143 total carbon contained in full diatoms ( $POC_{diat}$ ) by the mean mixed layer depth at the  
144 sampling time.

145 The export flux of diatoms was calculated using the equation:

$$146 \quad Cell\ flux = N_{diat} \times d \times 8 \times V_{aliquot} \times \frac{1}{0.125} \times \frac{1}{11} \times k$$

147 Where  $N_{diat}$  (cell  $m^{-2} d^{-1}$ ) is the number of cells counted in one chamber,  $d$  is the dilution  
148 factor,  $V_{aliquot}$  is the volume of the aliquot, and  $k$  is the fraction of the chamber counted.

149 The diatom flux was then converted to POC flux for each taxon using allometric equations.

### 150 **Biogeochemical analysis.**

151 Dissolved major nutrients ( $NO_3^-$  and  $Si(OH)_4$ ) in the RAS were measured in the 0.8  $\mu m$  filtered  
152 (polycarbonate filters ) samples preserved with mercuric chloride using standard protocols  
153 that have been previously applied to samples of this site (Blain et al. 2015).

### 154 **Community weighted mean (CWM) .**

155 CWM is defined using the equation

$$156 \quad CWM = \sum_{i=1}^N p_i \times C_{diat,i}$$

157 where for the taxa  $i$ ,  $p_i$  is its relative abundance and  $C_{diat,i}$  is its carbon content.

158 To estimate the effect of the variability of the diatom composition on the CWM we  
159 simulated virtual diatom communities. We first randomly selected 14 taxa among the 30  
160 taxa contributing to at least 1% of the biomass and then we allocated to these selected  
161 diatom taxa a random abundance ranging between 0 and their respective maximum  
162 abundance observed during the season. Finally  $N_t$  and CWM were calculated. The simulation  
163 was repeated 1000 times.

### 164 **Calculation of the critical cell concentrations.**

165 The critical cell concentration was calculated according to the equation of (Jackson 1990) .

166  $C_{Cr}(\text{cell } m^{-3}) = \frac{0.096 \times \mu}{\alpha \times \gamma \times ESR^3}$  where ESR is the Equivalent Spherical Radius (m),  $\mu$  is the net  
167 growth rate ( $s^{-1}$ ),  $\alpha$  is the stickiness and  $\gamma$  is the shear rate ( $s^{-1}$ ) estimated according to the  
168 formulation (MacKenzie and Leggett 1993).

169  $\gamma = \sqrt{\frac{\varepsilon}{\nu}}$  where  $\varepsilon = \left(\frac{\tau}{\rho_w}\right)^{3/2} \times \frac{1}{kZ}$

170  $\tau$  is the mean wind stress of  $0.22 \text{ Nm}^{-2}$  for the period of interest obtained from the Japanese  
171 55-yr reanalysis (JRA-55; available online at <http://jra.kishou.go.jp>).  $\nu$  is seawater kinematic  
172 viscosity ( $10^{-6} \text{ m}^2\text{s}^{-1}$ ),  $\rho_w$  is the seawater density in the mixed layer ( $1027 \text{ kg m}^{-3}$ ).  $k$  is the von  
173 Kármán constant (0.41) and  $Z$  is the mixed layer depth (70 m).

174 Simulations represented in SI Fig. 3 were obtained using the equations above with different  
175 values of  $\alpha$  (0.1, 0.25, 0.5 and 1) and  $\mu$  (0.05 and  $0.13 \text{ d}^{-1}$ ).

176

177 RESULTS

178 **Environmental context and temporal phytoplankton bloom dynamics**

179 The region of interest for our study is located south-east of Kerguelen island on the central  
180 part of the Kerguelen Plateau (Figure 1a). The sampling site is located in a zone that has  
181 been identified during previous studies in Jan-Feb 2005 (Blain et al. 2007) and Oct-Nov 2011  
182 (Blain et al. 2015) as the core of the Kerguelen bloom. The ocean colour satellite images for  
183 the season 2016-2017 confirm that the large bloom, typical of this region, was also present  
184 during the time period considered here. The temporal variations of surface chlorophyll in the  
185 vicinity of the sampling site show the succession of two blooms peaking in November and  
186 January (Figure 1B). This seasonal pattern is consistent with the dual blooms as revealed  
187 from the climatology for this site (Figure 1B). Ocean colour images combined with back-  
188 trajectories derived from current speeds and directions at 42 m (SI Figure 1) show that the  
189 horizontal advection of surface water parcels that reached the sampling site during a time  
190 step of 11 days did not result in large variability of chlorophyll. The influence of spatial  
191 variability was therefore limited and we will interpret changes observed at the sampling site  
192 as mainly resulting from temporal variability.

193 The seasonal changes of the mixed layer depth (MLD) show that all the samples collected by  
194 the RAS were located in the mixed layer (Figure 2A). The variation of diatom carbon biomass  
195 integrated over the mixed layer, which accounted for the surface biomass (Pellichero et al.  
196 2020), presented similar temporal variations to chlorophyll concentrations (Figure 2C). The  
197 build-up of diatom biomass affected the concentrations of major nutrients in surface waters  
198 (Figure 2D). The concentrations of nitrate and silicic acid were high at the beginning of the  
199 season and decreased during the first bloom. This decrease was much larger for silicic acid

200 than for nitrate. Silicic acid concentrations increased slightly after the first bloom before  
201 being further depleted after the second bloom.

202

### 203 **Temporal dynamics of surface diatom communities**

#### 204 **Main taxa contributing to carbon biomass**

205 Throughout the season, the Kerguelen blooms were dominated by diatoms (Lasbleiz et al.  
206 2016; Rembauville et al. 2017), in contrast to blooms in temperate regions where diatoms  
207 are replaced by other phytoplankton during part of the productive season (Barber and  
208 Hiscock 2006). For the RAS time series, diatoms accounted for  $89 \pm 9$  % of carbon  
209 phytoplankton biomass observed by microscopy supporting the idea of diatom dominance.  
210 Because we wanted to explore the relationship between biogeochemistry (carbon biomass  
211 and export) and composition of the diatom community, we describe the latter using  
212 microscopic observations rather than DNA sequencing. In this context, the advantages of  
213 microscopic observations are that they allow the taxonomic identification, the  
214 determination of absolute counts of full cells (i.e; containing carbon) and quantitative  
215 estimates of the carbon content ( $C_{\text{diat}}$ ) derived from size measurements (Hillebrand et al.  
216 1999; Menden-Deuer and Lessard 2000; Cornet-Barthau et al. 2007). In the following, we  
217 consider only diatoms at the genus or species level (hereafter referred to as taxa) that  
218 contribute to  $> 1\%$  of the total diatom C biomass ( $\text{POC}_{\text{diat}}$ ). In the mixed layer, we identified a  
219 total of 30 different taxa during the entire season (Fig. 2 b). The number of taxa was  
220 relatively constant throughout the season (min =11, max =15, median=14), whereas the  
221 composition of the community varied dramatically (Fig. 2B). The first peak of Chlorophyll and  
222  $\text{POC}_{\text{diat}}$  (Fig. 2c) was dominated by taxa with low  $C_{\text{diat}}$ , typically *Chaetoceros (Hyalochaete)*,  
223 *Thalassiosira antarctica*, including their resting spores, and other small centric diatoms. The

224 second maximum of Chlorophyll a and POC<sub>diat</sub> was dominated by taxa characterized by high  
225 C<sub>diat</sub> (*Eucampia antarctica*, *Corethron inerme*, *Ondotella weissflogii*, *Thalassiothrix*  
226 *antarctica*) with the exception of the pennate *Pseudo-nitzschia*, a genus commonly identified  
227 in artificially iron fertilized blooms (Marchetti et al. 2012). The iconic pennate species of the  
228 Southern Ocean *Fragilariopsis kerguelensis* had substantial contributions to POC<sub>diat</sub> in our  
229 first sample (25 October). Its contribution continuously decreased as the first bloom  
230 developed, became negligible during the second bloom and started to recover in late  
231 summer.

232

### 233 **Seasonal changes of abundance, size and carbon content.**

234 The abundance of the main diatom taxa (30 in total) contributing to the total carbon  
235 biomass POC<sub>diat</sub> varied by 3 orders of magnitude and their individual biovolumes varied by  
236 more than 3 orders of magnitude (from 112  $\mu\text{m}^3$  up to 152600  $\mu\text{m}^3$ ). To examine how these  
237 variations affect the total carbon biomass POC<sub>diat</sub>, we characterized the diatom communities  
238 observed at 12 time points during the season in two different manners.

239 In the first approach, we used the diatom community size spectrum. The slope of the size  
240 spectra revealed marked changes throughout the season (Table 1 and SI Fig. 2).

241 At the beginning of the season, the slope was within the range [-0.8,-0.7]. By mid-December  
242 which coincided with the end of the declining phase of the first bloom, the slope increased  
243 rapidly up to values in the range [-0.2,-0.3], and these values were maintained until the last  
244 week of February. These latter slopes were less significant due to one or two outliers located  
245 in the middle of the size-class range that could indicate a bi-modal distribution rather than a  
246 linear one. At the end of February, the slope increased to a value of -0.51.

247 If we consider that the biovolume scales with the diatom abundance, as shown by the size  
248 spectrum, and if the individual carbon content of diatoms scales with the biovolume as  
249 supported by previous studies (Menden-Deuer and Lessard 2000; Cornet-Barthau et al.  
250 2007), it is in principle possible to sum up the contributions of the different size classes to  
251 obtain the total carbon biomass  $POC_{diat}$  of the community. However, this approach could be  
252 biased if the contribution of diatom spores to a size class is non-negligible. Indeed, the  
253 volumetric carbon content of a spore is higher than that of a vegetative cell (Rembauville et  
254 al. 2015a).

255 For this reason we also characterized the diatom communities using a second approach and  
256 estimated the community weighted mean (CWM) (Fig. 3A). Obviously, the CWM and the  
257 total carbon biomass  $POC_{diat}$  are linked using the equation  $POC_{diat} = N_t \times CWM$  where  $N_t$  is the  
258 total abundance of diatoms of the community. CWM and  $N_t$  show clear opposite seasonal  
259 trends, increasing and decreasing, respectively, throughout the season (Fig. 3A, B). These  
260 changes provided insight to the seasonal variations of the total diatom carbon biomass.

261

### 262 **Coupling between diatom taxa in surface waters and their export**

263 The carbon fluxes attributed to diatoms in each cup of the sediment trap are presented in  
264 Fig. 4A. The first export event was mainly collected by cups #3, #4 and #5. The cumulated  
265 flux in these 3 cups was  $3.9 \text{ mmol C m}^{-2} \text{ d}^{-1}$  and it represented 60 % of the seasonal diatom  
266 carbon flux. The second event was recorded in cups # 9 and #10 and the corresponding  
267 cumulated flux was  $1.4 \text{ mmol C m}^{-2} \text{ d}^{-1}$  which accounted for 21% of the seasonal diatom  
268 carbon flux. The seasonal pattern of diatom carbon export was remarkably similar to those  
269 observed in 2011-2012 at the same site (Rembauville et al. 2015b).

270 The relative contributions of the different taxa to diatom carbon export are shown in Fig. 4B.  
271 The first event was entirely dominated by the export of *Chaetoceros* and *Thalassiosira*  
272 resting spores while more diverse taxa were contributing to the second event. For the latter,  
273 when cups #9 and #10 are cumulated, the relative contributions of the different taxa were:  
274 *Chaetoceros* resting spores (43%), *Pseudo-nitzschia heimii* (2%), *Pseudo-nitzschia lineola*  
275 (3%), *Navicula directa* (0.7%), *Eucampia antarctica* (20.4%), *Corethron inerme* (4.2%),  
276 *Odontella weisflogii* spores (15.3%), *Proboscia inermis* (1.3%), *Thalassiothrix antarctica*  
277 (3.6%), *Membraneis challenger* (5%), *Rhizosolenia styliformis* (1.5%), *Asteromphalus*  
278 *hookeri*(1.7%).

279 The synchronized sampling of diatom communities in the mixed layer and in the sediment  
280 traps (Fig. 2A) allowed a detailed investigation of the coupling between the dynamics of the  
281 abundance of individual diatom taxa in the mixed layer and of their export at 300 m. To  
282 compare both dynamics we calculated, for a given genus, its relative contribution at each  
283 time point to its total seasonal abundance and to its total seasonal export flux (Fig. 5).

284 It is evident that the maximum seasonal abundance of the different diatom genera in the  
285 mixed layer occurred during a short time period, closely followed by a carbon export event  
286 of the same genus. We observed that more than 44.2 % (for *Thalassionema*) and up to 100 %  
287 (for *Proboscia*) of the seasonal export attributable to a given genus took place during a  
288 relatively short time period, representing 17 % of the entire sampling period (132 days)  
289 (Table 2). To confirm the link between the dynamics of diatom surface abundance and  
290 export we estimated for each genus the correlation between the two time series with  
291 different time lags (SI Fig. 3). The correlation is significant for 10 of the genera, the  
292 exceptions being *Fragilariopsis* and *Odontella*. The time lag leading to the best correlation  
293 between both time series was 0 day for *Membraneis*, *Thalassiosira*, 11 days for *Proboscia*,

294 *Rhizosolenia*, *Eucampia*, *Thalassionema* and *Chaetoceros* and 22 days for *Corethron* and  
295 *Thalassiothrix*.

296

## 297 DISCUSSION

298 Our study was designed to address the coupling between the seasonal dynamics of diverse  
299 diatoms in the surface layer and their export at depth. Our major aim was to refine previous  
300 conceptual views both on a temporal scale and on the taxon level, and thereby to make an  
301 important step forward. Thanks to the seasonal coverage with good temporal resolution,  
302 and to the synchronized observations between the surface layer and at depth we are able to  
303 reveal a common pattern for diatom species belonging to 10 different genera that are short  
304 pulses of surface abundance followed by export.

305 Short-term artificial iron fertilization experiments in the Southern Ocean and more  
306 specifically the 35 days long EIFEX cruise (Smetacek et al. 2012) revealed the critical role of  
307 the pulsed nature of POC export due to boom-and-burst diatoms (Assmy et al. 2013)  
308 exemplified by *Chaetoceros dichaeta*. On a seasonal scale, the pulsed export of different  
309 diatom taxa was inferred from sediment trap deployments in the Australian sector of the  
310 Southern Ocean. The relative abundance of *Pseudo-nitzschia* and of the small *Fragilariopsis*  
311 spp. in sediment traps was closely related to POC pulses in the Polar Front and in the Sub  
312 Antarctic zones (Rigual-Hernández et al. 2016). Similar observations were made for  
313 *Fragilariopsis kerguelensis* and *Thalassiothrix antarctica* in the Antarctic zone (Rigual-  
314 Hernández et al. 2015). However, seasonal changes of the surface diatom communities were  
315 not described in these previous studies, limiting further investigation of the origin of these  
316 diatom pulses for carbon export. In addition, empty and full diatom cells were not  
317 distinguished by the methodology applied (Romero et al. 2000).



318 Our work provides evidences of the pulsed export of diatoms for additional diatom  
319 taxa, but it also allows us to go a step further and to address the question: what causes such  
320 a common pattern? To answer this question, we start with the examination of the seasonal  
321 changes of diatom abundance and size in the mixed layer. The maximum abundance reached  
322 during the season by diatoms belonging to 12 different genera was strongly related to size,  
323 characterized by the spherical equivalent radius (Fig 6 and SI Fig. 4).

324 Our simulation (Fig. 3D) shows that this unique constraint, that is size, produces an  
325 envelope of communities characterized by CWM and  $N_t$  consistent with the communities  
326 observed in situ.

327 The slopes of the size-class spectrum determined in our study at the beginning of the  
328 season were close to those reported for coastal eutrophic and upwelling ecosystems  
329 (around -0.8; Cermeño and Figueiras 2008), while slopes up to -1.3 are reported for  
330 subtropical regions (Cermeño and Figueiras 2008). A 10 year time series at a shelf station in  
331 a temperate region revealed little variation (-0.96), with only episodically low slopes (-0.6)  
332 during the relaxation of upwelling (Huete-Ortega et al. 2010). In comparison, the slopes  
333 obtained in the present study during the second part of the season (-0.29 to -0.25) are low.  
334 Both, the changes of the slope of the size-class spectrum (Table 1) and of the CWM are  
335 explained by the replacement of small and abundant diatoms during the first part of the  
336 season by large and less abundant diatoms during summer.

337 The paradigm that small phytoplankton dominate when resources are limited, as is  
338 typically the case in oligotrophic gyres, and that large cells thrive when sufficient amounts of  
339 resources are available, typical for coastal environments or upwelling regions, has been  
340 invoked to explain spatial differences in the slopes of the phytoplankton community size  
341 spectrum and can be explained by the size scaling of nutrient requirements and growth

342 (Irwin et al. 2006). Our observations that large cells dominate in summer when essential  
343 nutrients like silicic acid (Fig. 2D) and iron (Blain et al. 2008) are at their lowest values seems  
344 at odds with this explanation. Therefore, another mechanism should control the size  
345 distribution of the diatom communities in this region. We propose the formation of diatom  
346 aggregates as an explanation. The first observations of diatom aggregates have been  
347 reported by (Billett et al. 1983; Smetacek 1985). Theoretical approaches have shown that  
348 the formation of aggregates occurs when a critical cell abundance is reached for given  
349 environmental and cell properties (Jackson 1990) and such predictions have been confirmed  
350 in situ (Boyd et al. 2002). The critical abundances calculated by Jackson's model were also  
351 consistent with POC and biovolumes determined at the Bermuda Atlantic time series and off  
352 southern California (Jackson and Kiørboe 2008). In the Kerguelen bloom the formation of  
353 aggregates has been suggested to occur during the spring bloom based on in situ  
354 observations of changes in the size spectrum and modelling (Jouandet et al. 2014). The  
355 critical abundance depends on both, the properties of diatoms (ESR, stickiness, and net  
356 growth rate) and the properties of the environment (shear rate). When applying our data to  
357 an aggregation model (Jackson 1990), it showed that the observed maximum abundances  
358 for individual taxa (Fig. 6), or for size classes (SI Fig. 4) was determined by the net-growth  
359 rate and the stickiness of individual diatom taxa.

360

361         If we look at the results of the model considering different stickiness values, a parameter  
362 that can vary largely depending on the taxa (Kiørboe et al. 1990), the agreement between the  
363 model and the data is better with  $\alpha=1$  for small cells ( $\mu=0.13 \text{ d}^{-1}$ ). The maximum abundances are  
364 even below the critical abundances predicted by the model with this value of  $\alpha$ . It is conceivable  
365 that the ESR of small cells is underestimated in the context of the formation of aggregates

366 because it does not take into account the presence of spines, which likely increase the ESR. For  
367 the larger cell (or size classes), that were growing around  $\mu=0.05 \text{ d}^{-1}$ , the better fitting is  
368 obtained for values of  $\alpha$  in the range 0.5-0.25 (Fig. 6 and SI Fig. 4). This suggests that the  
369 stickiness of these larger cells would be lower. These results obtained at the diatom taxon  
370 level extend the previous conclusion of Jackson and Kjørboe 2008 obtained for bulk POC that  
371 the formation of diatom aggregates is a major factor of control for the maximum diatom  
372 abundance and consequently for their export.

373         When aggregates formed in the mixed layer are exported below the mixed layer  
374 depth, pulsed export events are expected. This was obviously the case considering the  
375 pulsed export dynamics observed in the present study (Fig. 5). We note that a similar  
376 seasonal pattern of carbon diatom export was observed in 2011-2012 at the same site  
377 (Rembauville et al. 2015a) suggesting that there is little interannual variability in the shape  
378 and magnitude of the carbon fluxes transported by diatoms. However, in the present study  
379 the total seasonal flux of POC was roughly 10 times higher than in 2011-2012 suggesting a  
380 large interannual variability in the carbon export due to faecal pellets. This observation is  
381 puzzling and advocates for seasonal monitoring of the composition of zooplankton  
382 community composition. Such observations were technically not feasible during the present  
383 study, but the rapid ongoing technological developments of underwater video profilers  
384 integrated to profiling floats (Claustre et al. 2020) or moorings provide promising  
385 perspectives for the near future.

386         Our sediment trap samples were collected using cups filled with hypersaline  
387 solution, and transported back to the laboratory for processing, including splitting. This  
388 protocol is not as well adapted to preserve aggregates as the collection and direct  
389 observation with gel traps (Ebersbach and Trull 2008). Considering the different estimates of

390 time lags we can also estimate the sinking velocity of aggregates. These are in the range 25  
391 to 250 m d<sup>-1</sup> and thus in good agreement with values determined in rolling tanks for  
392 aggregates formed with different Southern Ocean diatoms ([13- 260 m d<sup>-1</sup>]; Laurenceau-  
393 Cornec et al. 2015).

394 Collectively, our observations let us conclude that the formation of diatom  
395 aggregates occurs throughout the season, and is driven by a threshold in the abundance of a  
396 given diatom taxon. This leads to pulsed temporal dynamics in the abundance of diatoms  
397 with diverse morphology and their export to depth. The control of the maximum abundance  
398 of a given diatom by the formation of aggregates drives the seasonal change in the slope of  
399 the size-class distribution of the diatom community. It also constrains the total carbon  
400 diatom biomass in a narrow range of values due to the inverse relationship between  $N_t$  and  
401 CWM.

402

403

404 References

- 405 Allen, A. E., C. L. Dupont, M. Oborník, and others. 2011. Evolution and metabolic significance of the  
406 urea cycle in photosynthetic diatoms. *Nature* **473**: 203.
- 407 Allen, C. S., J. Pike, C. J. Pudsey, and A. Leventer. 2005. Submillennial variations in ocean conditions  
408 during deglaciation based on diatom assemblages from the southwest Atlantic: diatom  
409 record from the falkland through. *Paleoceanography* **20**: n/a-n/a.  
410 doi:10.1029/2004PA001055
- 411 Armand, L. K., X. Crosta, B. Quéguiner, J. Mosseri, and N. Garcia. 2008. Diatoms preserved in surface  
412 sediments of the northeastern Kerguelen Plateau. *Deep Sea Research Part II: Topical Studies*  
413 *in Oceanography* **55**: 677.
- 414 Armbrust, A. V., J. A. Berges, C. Bowler, and others. 2004. The genome of th diatom *Thalassiosira*  
415 *pseudonana*: ecology, evolution and metabolism. *Science* **306**: 79–86.
- 416 Armbrust, E. V. 2009. The life of diatoms in the world's oceans. *Nature* **459**: 185–192.  
417 doi:10.1038/nature08057
- 418 Assmy, P., V. Smetacek, M. Montresor, and others. 2013. Thick-shelled, grazer-protected diatoms  
419 decouple ocean carbon and silicon cycles in the iron-limited Antarctic Circumpolar Current.  
420 *Proceedings of the National Academy of Sciences* **110**: 20633–20638.  
421 doi:10.1073/pnas.1309345110
- 422 Barber, R. T., and M. R. Hiscock. 2006. A rising tide lifts all phytoplankton: Growth response of other  
423 phytoplankton taxa in diatom-dominated blooms: A RISING TIDE RAISES ALL  
424 PHYTOPLANKTON. *Global Biogeochem. Cycles* **20**: n/a-n/a. doi:10.1029/2006GB002726
- 425 Billett, D. S. M., R. S. Lampitt, A. L. Rice, and R. F. C. Mantoura. 1983. Seasonal sedimentation of  
426 phytoplankton to the deep-sea benthos. *Nature* **302**: 520–522. doi:10.1038/302520a0
- 427 Blain, S., J. Capparos, A. Guéneuguès, I. Obernosterer, and L. Oriol. 2015. Distributions and  
428 stoichiometry of dissolved nitrogen and phosphorus in the iron-fertilized region near  
429 Kerguelen (Southern Ocean). *Biogeosciences* **12**: 623–635. doi:10.5194/bg-12-623-2015

430 Blain, S., B. Quéguiner, L. Armand, and others. 2007. Effect of natural iron fertilisation on carbon  
431 sequestration in the Southern Ocean. *Nature* **446**: 1070–1075. doi:doi:10.1038/nature05700

432 Blain, S., G. Sarthou, and P. Laan. 2008. Distribution of dissolved iron during the natural iron-  
433 fertilization experiment KEOPS (Kerguelen Plateau, Southern Ocean). *Deep Sea Research Part*  
434 *II: Topical Studies in Oceanography* **55**: 594.

435 Boyd, P. W., G. A. Jackson, and A. M. WAite. 2002. Are mesoscale perturbation experiments in polar  
436 waters prone to physical artefacts? Evidence from algal aggregation modelling studies.  
437 *Geophysical Research Letters* **20**: doi: 10.1029/2001GL014210.

438 Cermeño, P., and F. Figueiras. 2008. Species richness and cell-size distribution: size structure of  
439 phytoplankton communities. *Mar. Ecol. Prog. Ser.* **357**: 79–85. doi:10.3354/meps07293

440 Claustre, H., K. S. Johnson, and Y. Takeshita. 2020. Observing the Global Ocean with Biogeochemical-  
441 Argo. *Annu. Rev. Mar. Sci.* **12**: 23–48. doi:10.1146/annurev-marine-010419-010956

442 Cornet-Barthau, V., L. Armand, and B. Quéguiner. 2007. Biovolume and biomass estimates of key  
443 diatoms in the Southern Ocean. *Aquatic Microbial Ecology* **48**: 295–308.

444 Crawford, R. M., F. Hinz, and T. Rynearson. 1997. Spatial and temporal distribution of assemblages of  
445 the diatom *Corethron criophilum* in the Polar Frontal region of the South Atlantic. *Deep Sea*  
446 *Research Part II: Topical Studies in Oceanography* **44**: 479.

447 Ebersbach, F., and T. Trull. 2008. Sinking particle properties from polyacrylamide gels during KEOPS:  
448 zooplankton control of carbon export in an area of persistent natural iron inputs in the  
449 Southern Ocean. *Limnology and Oceanography* **53**: 212–224.

450 Gall, M. P., R. Strzepek, M. Maldonado, and P. W. Boyd. 2001. Phytoplankton processes. Part 2: Rates  
451 of primary production and factors controlling algal growth during the Southern Ocean Iron  
452 RElease Experiment (SOIREE). *Deep Sea Research Part II: Topical Studies in Oceanography* **48**:  
453 2571.

454 Hamm, C., and V. Smetacek. 2007. Armor: Why, When, and How, p. 311–332. *In* *Evolution of Primary*  
455 *Producers in the Sea*. Elsevier.

456 Hillebrand, H., C.-D. Dürselen, D. Kirschtel, U. Pollinger, and T. Zohary. 1999. Biovolume calculation  
457 for pelagic and benthic microalgae. *Journal of Phycology* **35**: 403–424. doi:10.1046/j.1529-  
458 8817.1999.3520403.x

459 Huete-Ortega, M., E. Maranon, M. Varela, and A. Bode. 2010. General patterns in the size scaling of  
460 phytoplankton abundance in coastal waters during a 10-year time series. *Journal of Plankton*  
461 *Research* **32**: 1–14. doi:10.1093/plankt/fbp104

462 Irwin, A. J., Z. V. Finkel, O. M. E. Schofield, and P. G. Falkowski. 2006. Scaling-up from nutrient  
463 physiology to the size-structure of phytoplankton communities. *Journal of Plankton Research*  
464 **28**: 459–471. doi:10.1093/plankt/fbi148

465 Jackson, G. A. 1990. A model of the formation of marine algal flocs by physical coagulation processes.  
466 *Deep Sea Research Part A. Oceanographic Research Papers* **37**: 1197–1211.  
467 doi:10.1016/0198-0149(90)90038-W

468 Jackson, G. A., and T. Kiørboe. 2008. Maximum phytoplankton concentrations in the sea. *Limnol.*  
469 *Oceanogr.* **53**: 395–399. doi:10.4319/lo.2008.53.1.0395

470 Jouandet, M.-P., G. A. Jackson, F. Carlotti, M. Picheral, L. Stemann, and S. Blain. 2014. Rapid  
471 formation of large aggregates during the spring bloom of Kerguelen Island: observations and  
472 model comparisons. *Biogeosciences* **11**: 4393–4406. doi:10.5194/bg-11-4393-2014

473 Katz, M. E., J. D. Wright, K. G. Miller, B. S. Cramer, K. Fennel, and P. G. Falkowski. 2005. Biological  
474 overprint of the geological carbon cycle. *Marine Geology* **217**: 323–338.  
475 doi:10.1016/j.margeo.2004.08.005

476 Kemp, A. E. S., R. B. Pearce, I. Grigorov, J. Rance, C. B. Lange, P. Quilty, and I. Salter. 2006. Production  
477 of giant marine diatoms and their export at oceanic frontal zones: Implications for Si and C  
478 flux from stratified oceans. *Global Biogeochemical Cycles* **20**. doi:10.1029/2006GB002698

479 Kiørboe, T., K. P. Andersen, and H. G. Dam. 1990. Coagulation efficiency and aggregate formation in  
480 marine phytoplankton. *Mar. Biol.* **107**: 235–245. doi:10.1007/BF01319822

481 Korb, R., M. Whitehouse, A. Atkinson, and S. Thorpe. 2008. Magnitude and maintenance of the  
482 phytoplankton bloom at South Georgia: a naturally iron-replete environment. *Mar. Ecol.*  
483 *Prog. Ser.* **368**: 75–91. doi:10.3354/meps07525

484 Lasbleiz, M., K. Leblanc, L. K. Armand, U. Christaki, C. Georges, I. Obernosterer, and B. Quéguiner.  
485 2016. Composition of diatom communities and their contribution to plankton biomass in the  
486 naturally iron-fertilized region of Kerguelen in the Southern Ocean G. King [ed.]. *FEMS*  
487 *Microbiology Ecology* **92**: fiw171. doi:10.1093/femsec/fiw171

488 Laurenceau-Cornec, E., T. Trull, D. Davies, C. De La Rocha, and S. Blain. 2015. Phytoplankton  
489 morphology controls on marine snow sinking velocity. *Marine Ecology Progress Series* **520**:  
490 35–56. doi:10.3354/meps11116

491 Leblanc, K., C. E. Hare, P. W. Boyd, and others. 2005. Fe and Zn effects on the Si cycle and diatom  
492 community structure in two contrasting high and low-silicate HNLC areas. *Deep Sea Research*  
493 *Part I: Oceanographic Research Papers* **52**: 1842–1864. doi:10.1016/j.dsr.2005.06.005

494 MacKenzie, B. R., and W. C. Leggett. 1993. Wind-based models for estimating the dissipation rates of  
495 turbulent energy in aquatic environments: empirical comparisons. *Marine Ecology Progress*  
496 *Series* **94**: 207–216.

497 Malviya, S., E. Scalco, S. Audic, and others. 2016. Insights into global diatom distribution and diversity  
498 in the world's ocean. *Proceedings of the National Academy of Sciences* **113**: E1516–E1525.  
499 doi:10.1073/pnas.1509523113

500 Marchetti, A., D. M. Schruth, C. A. Durkin, and others. 2012. Comparative metatranscriptomics  
501 identifies molecular bases for the physiological responses of phytoplankton to varying iron  
502 availability. *Proceedings of the National Academy of Sciences* **109**: E317–E325.  
503 doi:10.1073/pnas.1118408109

504 Margalef, R. 1978. Life-form of phytoplankton as survival alternatives in an unstable environment.  
505 *Oceanologica Acta* **1**: 493–509.



506 Menden-Deuer, S., and E. J. Lessard. 2000. Carbon to volume relationships for dinoflagellates,  
507 diatoms, and other protist plankton. *Limnol. Oceanogr.* **45**: 569–579.  
508 doi:10.4319/lo.2000.45.3.0569

509 Nelson, D. M., P. Tréguer, M. A. Brzezinski, A. Leynaert, and B. Quéguiner. 1995. Production and  
510 dissolution of biogenic silica in the ocean: Revised global estimates, comparison with regional  
511 data and relationship to biogenic sedimentation. *Global Biogeochem. Cycles* **9**: 359–372.  
512 doi:10.1029/95GB01070

513 Pellichero, V., J. Boutin, H. Claustre, L. Merlivat, J. Sallée, and S. Blain. 2020. Relaxation of Wind Stress  
514 Drives the Abrupt Onset of Biological Carbon Uptake in the Kerguelen Bloom: A Multisensor  
515 Approach. *Geophys. Res. Lett.* **47**. doi:10.1029/2019GL085992

516 Quéguiner, B. 2013. Iron fertilization and the structure of planktonic communities in high nutrient  
517 regions of the Southern Ocean. *Deep Sea Research Part II: Topical Studies in Oceanography*  
518 **90**: 43–54. doi:10.1016/j.dsr2.2012.07.024

519 Queguiner, B., P. Treguer, I. Peeken, and R. Scharek. 1997. Biogeochemical dynamics and the silicon  
520 cycle in the Atlantic sector of the Southern Ocean during austral spring 1992. *Deep Sea*  
521 *Research Part II: Topical Studies in Oceanography* **44**: 69.

522 Raven, J. A., and A. M. Waite. 2004. The evolution of silicification in diatoms: inescapable sinking and  
523 sinking as escape? *New Phytol* **162**: 45–61. doi:10.1111/j.1469-8137.2004.01022.x

524 Rembauville, M., S. Blain, L. Armand, B. Quéguiner, and I. Salter. 2015a. Export fluxes in a naturally  
525 iron-fertilized area of the Southern Ocean – Part 2: Importance of diatom resting spores and  
526 faecal pellets for export. *Biogeosciences* **12**: 3171–3195. doi:10.5194/bg-12-3171-2015

527 Rembauville, M., N. Briggs, M. Ardyna, and others. 2017. Plankton Assemblage Estimated with BGC-  
528 Argo Floats in the Southern Ocean: Implications for Seasonal Successions and Particle Export:  
529 *Journal of Geophysical Research: Oceans* **122**: 8278–8292. doi:10.1002/2017JC013067

530 Rembauville, M., I. Salter, N. Leblond, A. Gueneugues, and S. Blain. 2015b. Export fluxes in a naturally  
531 iron-fertilized area of the Southern Ocean – Part 1: Seasonal dynamics of particulate organic

532 carbon export from a moored sediment trap. *Biogeosciences* **12**: 3153–3170.  
533 doi:10.5194/bg-12-3153-2015

534 Rigual-Hernández, A. S., T. W. Trull, S. G. Bray, and L. K. Armand. 2016. The fate of diatom valves in  
535 the Subantarctic and Polar Frontal Zones of the Southern Ocean: Sediment trap versus  
536 surface sediment assemblages. *Palaeogeography, Palaeoclimatology, Palaeoecology* **457**:  
537 129–143. doi:10.1016/j.palaeo.2016.06.004

538 Rigual-Hernández, A. S., T. W. Trull, S. G. Bray, I. Closset, and L. K. Armand. 2015. Seasonal dynamics  
539 in diatom and particulate export fluxes to the deep sea in the Australian sector of the  
540 southern Antarctic Zone. *Journal of Marine Systems* **142**: 62–74.  
541 doi:10.1016/j.jmarsys.2014.10.002

542 Romero, O. E., G. Fischer, C. B. Lange, and G. Wefer. 2000. Siliceous phytoplankton of the western  
543 equatorial Atlantic: sediment traps and surface sediments. *Deep Sea Research Part II: Topical  
544 Studies in Oceanography* **47**: 1939–1959. doi:10.1016/S0967-0645(00)00012-6

545 Salter, I., A. E. S. Kemp, C. M. Moore, R. S. Lampitt, G. A. Wolff, and J. Holtvoeth. 2012. Diatom resting  
546 spore ecology drives enhanced carbon export from a naturally iron-fertilized bloom in the  
547 Southern Ocean. *Global Biogeochemical Cycles* **26**. doi:10.1029/2010GB003977

548 Smetacek, V., C. Klaas, V. H. Strass, and others. 2012. Deep carbon export from a Southern Ocean  
549 iron-fertilized diatom bloom. *Nature* **487**: 313–319. doi:10.1038/nature11229

550 Smetacek, V. S. 1985. Role of sinking in diatom life-history cycles: ecological, evolutionary and  
551 geological significance. *Marine Biology* **84**: 239–251. doi:10.1007/BF00392493

552 Tréguer, P., C. Bowler, B. Moriceau, and others. 2018. Influence of diatom diversity on the ocean  
553 biological carbon pump. *Nature Geoscience* **11**: 27–37. doi:10.1038/s41561-017-0028-x

554 Tremblay, J. E., M. I. Lucas, G. Kattner, R. Pollard, V. H. Strass, U. Bathmann, and A. Bracher. 2002.  
555 Significance of the Polar Frontal Zone for large-sized diatoms and new production during  
556 summer in the Atlantic sector of the Southern Ocean. *Deep Sea Research Part II: Topical  
557 Studies in Oceanography* **49**: 3793.

558 **Table 1** : Seasonal changes of diatom communities size class spectrum parameters where  
 559 biovolume were in  $\mu\text{m}^3$  and abundance in cell  $\text{L}^{-1}$

date	sample	slope	intercept	R_squared	p
10/25/2016	1	-0.81	7.001	0.563	0.012
11/06/2016	2	-0.82	7.683	0.529	0.017
11/17/2016	3	-0.73	7.225	0.732	0.003
11/28/2016	4	-0.71	7.082	0.745	0.002
12/09/2016	5	-0.50	6.309	0.559	0.020
12/20/2016	6	-0.48	5.801	0.270	0.123
12/31/2016	7	-0.20	5.111	0.040	0.577
01/11/2017	8	-0.25	5.413	0.120	0.360
01/22/2017	9	-0.25	5.214	0.175	0.262
02/02/2017	10	-0.22	5.067	0.361	0.115
02/13/2017	11	-0.19	4.577	0.102	0.400
02/24/2017	12	-0.51	5.731	0.400	0.090

560

561

562 **Table 2 : Diatom taxa, and biological and environmental parameters**

Diatoms	% <sup>a</sup>	Morphology <sup>b</sup>	Spores	$\mu^c$ d <sup>-1</sup>	T max <sup>d</sup>	Si(OH <sub>4</sub> ) <sup>e</sup> $\mu$ M	NO <sub>3</sub> <sup>e</sup> $\mu$ M
<i>Proboscia inermis</i>	100	CR	N		7	3.18	22.1
<i>Membraneis challengerii</i>	84.3	PRap	N		10	2.45	22.8
<i>Thalassiosira antarctica</i>	78.7	CR	Y	0.17	2	17.9	25.4
<i>Thalassiothrix antarctica</i>	77.2	PARap	N		7	3.18	22.1
<i>Rhizosolenia chunii</i>	76.6	CR	N		7	3.18	22.1
<i>Pseudo-nitzschia spp.</i>	68.1	PRap	N	0.067	7	3.18	22.1
<i>Eucampia antarctica</i>	67.1	CMP	Y	0.072	7	3.18	22.1
<i>Corethron inerme</i>	65.3	CR	N	0.046	7	3.18	22.1
<i>Odontella weisflogii</i>	63.4	CMP	Y		7	3.18	22.1
<i>Chaetoceros (Hyalochaete)</i>	59.6	CMP	Y	0.13	2	17.9	25.4
<i>Navicula directa</i>	58.4	PRap	N		8	4.52	21.9
<i>Fragilariopsis kerguelensis</i>	49.6	PRap	N	0.077	2	17.9	22.8
<i>Thalassionema nitzschioides</i>	44.2	PRap	N	0.11	2	17.9	22.8

563

564 <sup>a</sup> percentage of the seasonal export achieved during the periods denoted with stars in Figure  
565 3

566 <sup>b</sup> CR centric radial, PRap Pennate raphid, CMP centric multipolar

567 <sup>c</sup> net growth rate determined from the increase in cell abundance during the growing phase  
568 of the population.

569 Spores: indicates whether diatom species produces spores (Y) or not (N)

570 <sup>d</sup> sample number when the abundance was maximum.

571 <sup>e</sup> Concentrations in  $\mu$ mol L<sup>-1</sup>

572

573

574

575 **List of figure legends:**

576

577 **Figure 1:** Chlorophyll seasonal changes and location of the mooring site. (A) Global view of  
578 the mooring site on the central Kerguelen plateau. The white dot denotes the position of the  
579 RAS mooring overlaying monthly chlorophyll for November 2016. The white rectangle  
580 denotes the zone that is detailed in the SI Figure 1. (B) The green line presents the  
581 climatology (1998-2017) at the mooring site with standard deviation represented with the  
582 light green shaded area. The blue line represents the chlorophyll concentrations from 8-days  
583 color satellite images at the same site for the period extending from Oct 2016 to April 2017.  
584 The vertical dotted line denotes the sampling dates.

585 **Figure 2:** Seasonal changes in the Kerguelen bloom. (A) The synchronized sampling strategy  
586 was based on an autonomous sampler collecting water in the mixed layer at 42 m and a  
587 sediment trap deployed at 300 m collecting the sinking flux. The stars denote dates when  
588 phytoplankton samples were collected. The white rectangles along the x axis, numbered 1 to  
589 12, are the periods of collection in the sediment trap cup. (B) Relative contribution of the  
590 different diatoms to the total diatom carbon biomass ( $POC_{diat}$ ) at 42 m. Diatoms are ordered  
591 according to their carbon content (SI 5 Data). Abbreviations for genus names are  
592 *Asteromphalus (A.)*, *Corethron (C.)*, *Chaetoceros (Ch.)*, *Eucampia (E.)*, *Fragilariopsis (F.)*,  
593 *Guinardia (G.)*, *Membraneis (M.)*, *Navicula (N.)*, *Odontella (O.)*, *Proboscia (P.)*, *Pseudo-*  
594 *nitzschia (P.\*)*, *Rhizosolenia (R.)*, *Thalassiothrix (T.\*)*, *Thalassiosira (T.)*, *Thalassionema (T.#)*.  
595 (C) integrated  $POC_{diat}$  in the mixed layer (black bars). The white circles denote the surface  
596 chlorophyll concentrations derived from 8 day composite images. (D) Silicic acid (white  
597 circle) and nitrate (grey square) concentrations measured in the filtered samples collected  
598 with RAS at 42 m.

599 **Figure 3:** Seasonal changes of diatom abundance in relation to carbon biomass.  
600 (A) Community Weighted Mean (B) total abundance (C) total carbon biomass. For all the  
601 plots the dots denote the value estimated from observation and the boxplot (median, first  
602 and third quartile) visualize the variability of the estimates based on 1000 simulations of  
603 diatom community assuming a normal distribution of the traits around the observed value  
604 with a variation coefficient of 0.5. (D) Diatom abundance ( $N_t$ ) versus CWM for 1000  
605 communities resulting from random composition and abundance of the different species  
606 according to observations (see methods for details). The black line represent the fitting of  
607 the equation  $N_t = \text{POC}_{\text{diat}} / \text{CWM}$  with  $\text{POC}_{\text{diat}} = 0.097 \text{ mg L}^{-1}$ .

608 **Figure 4 : Carbon export fluxes by diatoms.** A) Total diatom carbon flux in each cup B) relative  
609 contribution of different taxa to total diatom carbon flux in each cup. Abbreviations for genus  
610 names are *Asteromphalus* (A.), *Corethron* (C.), *Eucampia* (E.), *Fragilariopsis* (F.), *Membraneis*  
611 (*M.*), *Navicula* (N.), *Odontella* (O.), *Proboscia* (P.), *Pseudo-nitzschia* (P.\*), *Rhizosolenia* (R.),  
612 *Thalassiothrix* (T.\*), *Thalassiosira* (T.), *Thalassionema* (T.#).

613 **Figure 5 :** Temporal changes in the relative contribution to the cumulated seasonal  
614 abundance of a given taxon (upper panels), and to the carbon export flux of the same taxon  
615 (lower panels). Vegetative cells are shown in black and spores are presented in gray. For  
616 clarity, only 1 tick every 2 cups is presented and only cup numbers 2, 6 and 10 are labeled.

617 **Figure 6 :** Comparison of the maximum seasonal abundances of the different diatom taxa  
618 (white circles), with the critical abundance derived from the aggregation model of Jackson.  
619 The shaded areas represent all the possible critical abundances considering different  
620 combinations of  $\mu$  and  $\alpha$  as indicated on the right y-axis.

621

622

623 ACKNOWLEDGMENT

624 We thank the captains and the crew of the R/V *Marion Dufresne* for their support during the  
625 cruises. We thank E. de Saint Léger, F. Pérault and L. Scoarnec from DT-INSU, and people of  
626 IPEV (Institut Polaire Paul Emile Victor) for the technical support during preparation,  
627 deployment and recovery of moorings. We also thanks Tom Trull who inspired the use of  
628 RAS for our project and Diana Davis for her valuable advises in the preparation of this  
629 equipment. We thanks the associate editor S. Menden-Deuer and the 4 anonymous  
630 reviewers for their constructive comments. This work is part of the project SOCLIM  
631 supported by the Climate Initiative of the foundation BNP Paribas, the French research  
632 program LEFE-CYBER of INSU-CNRS, IPEV, Sorbonne Université, and the Flotte  
633 Océanographique Française. The authors declare no conflict of interest.

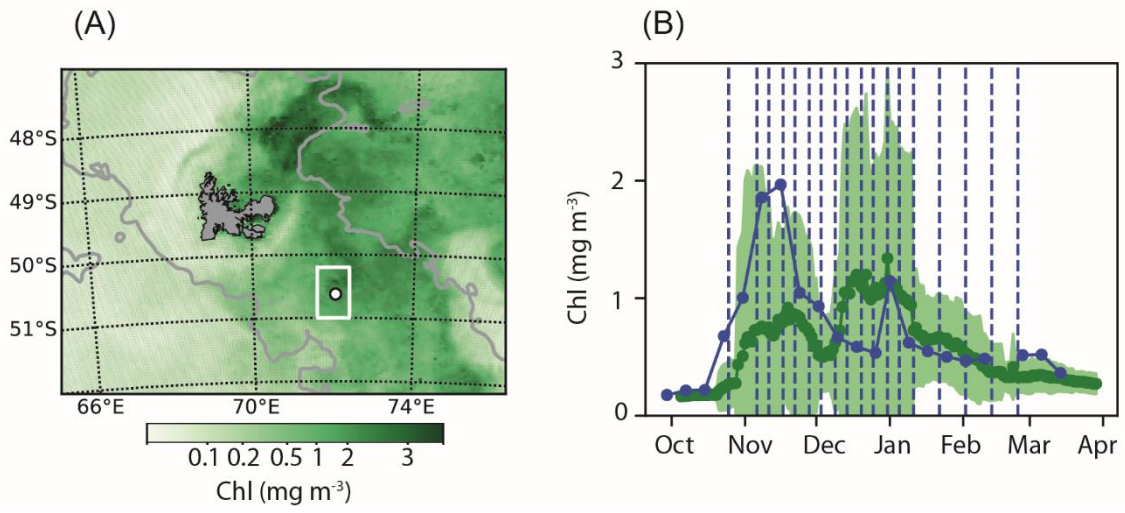


Figure 1



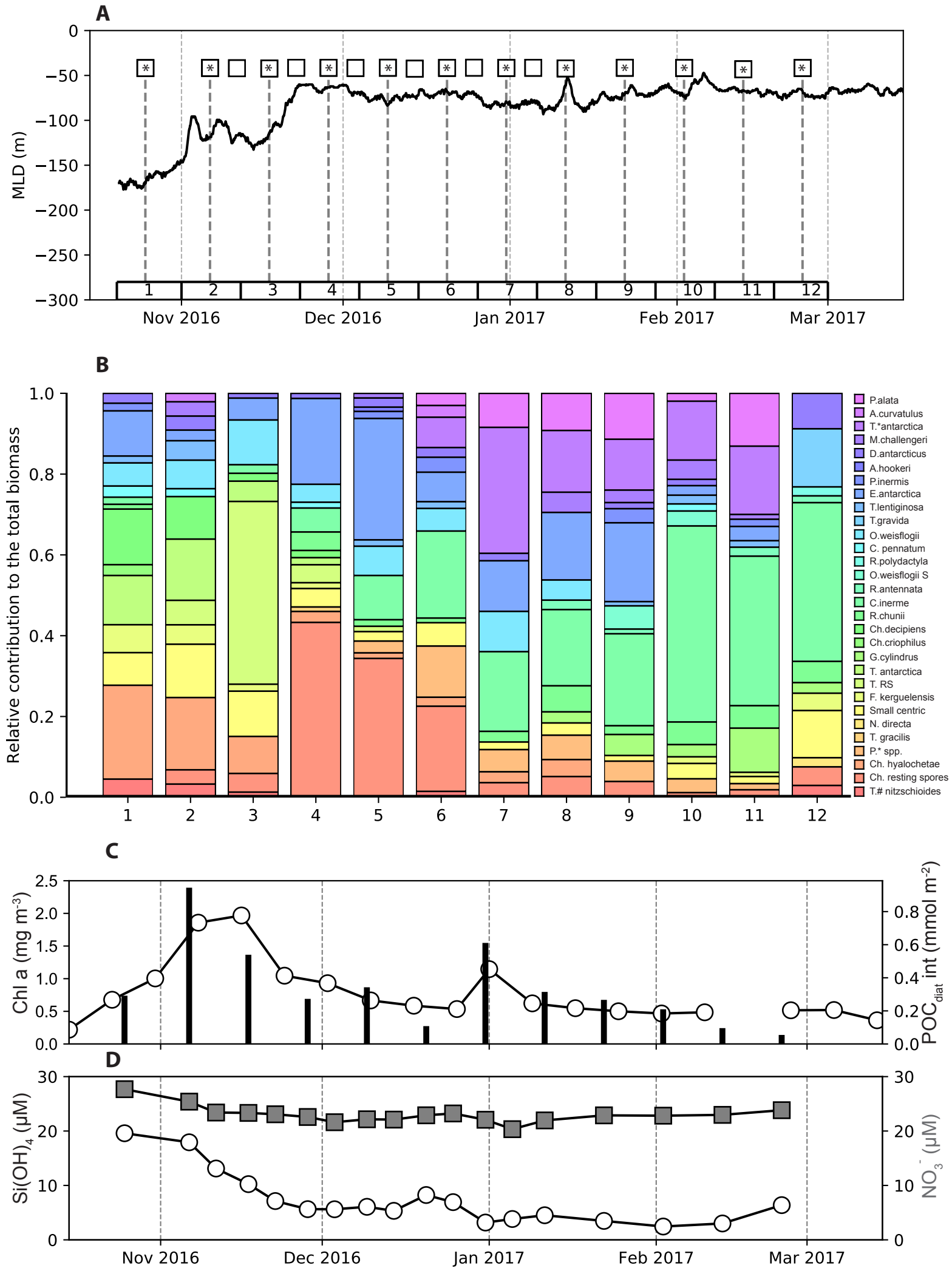


Figure 2

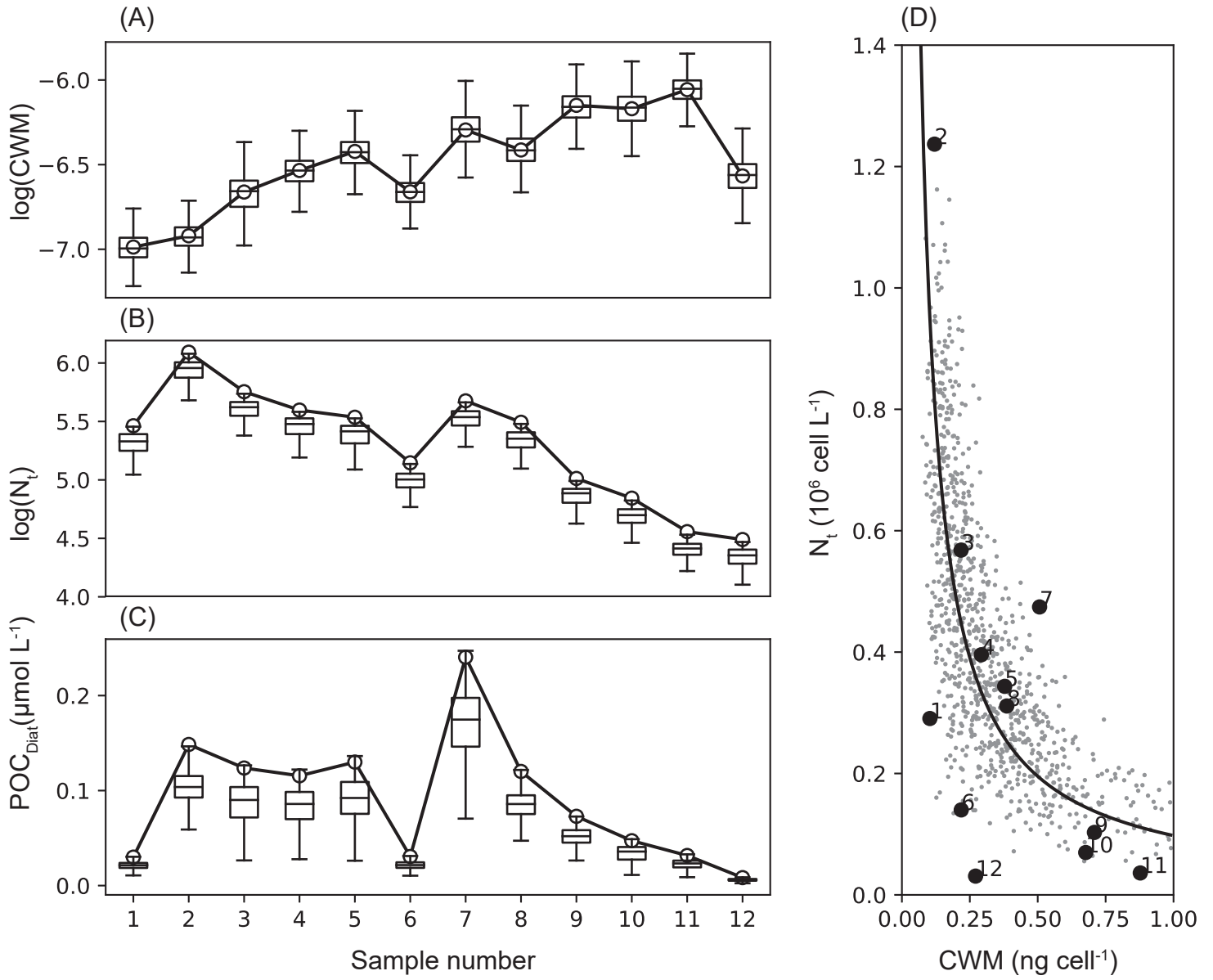


Figure 3

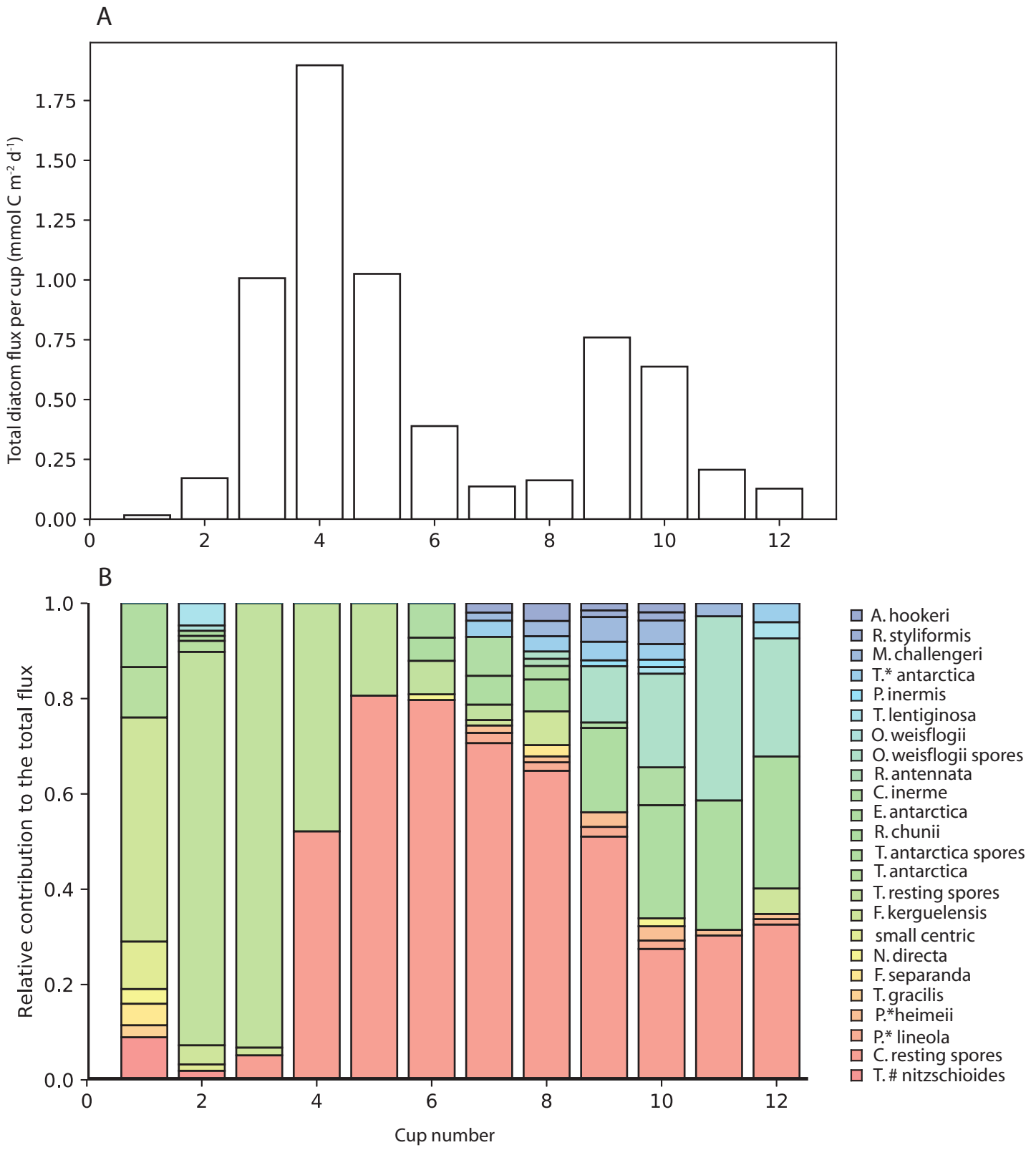


Figure 4

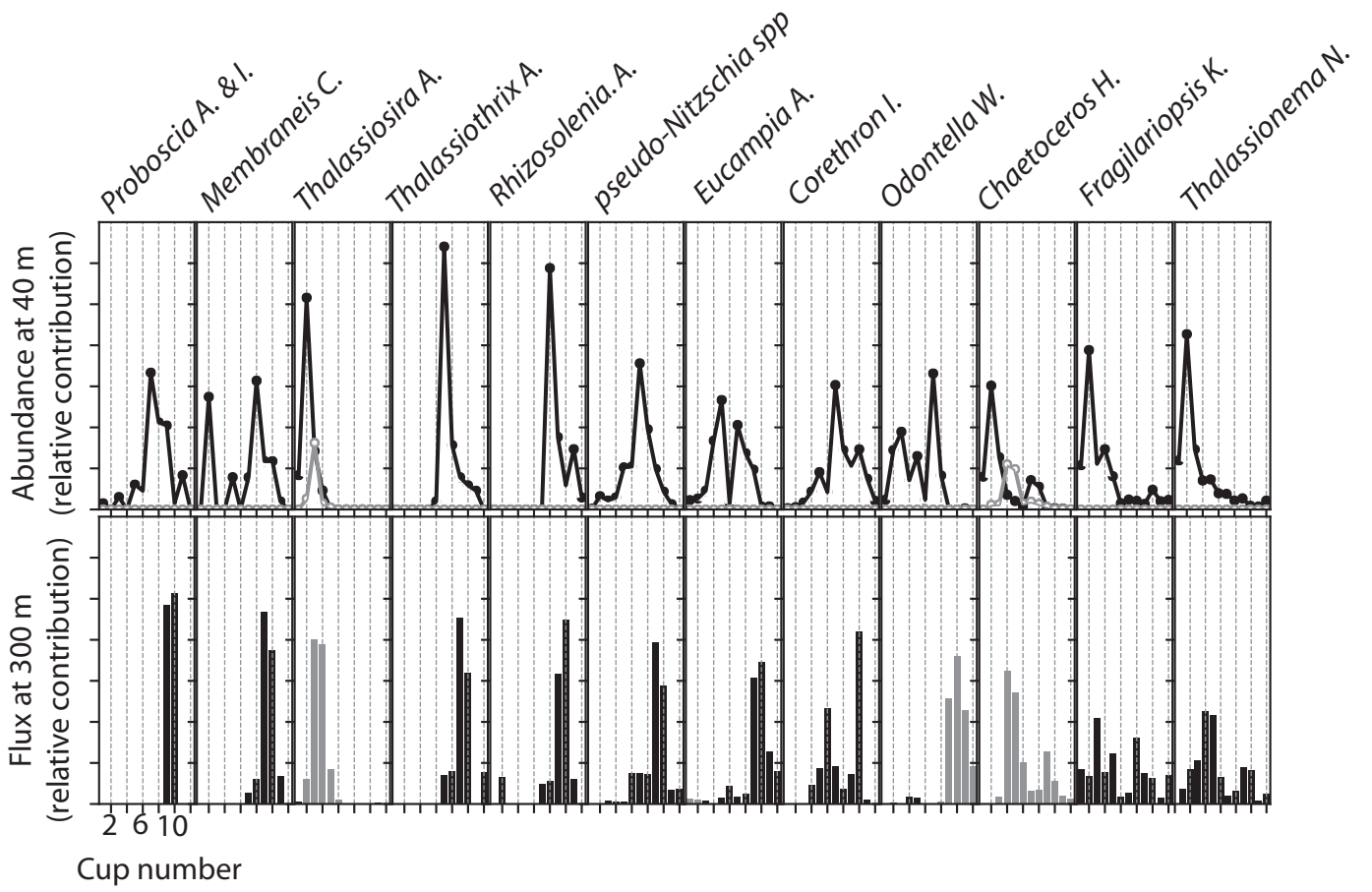


Figure 5

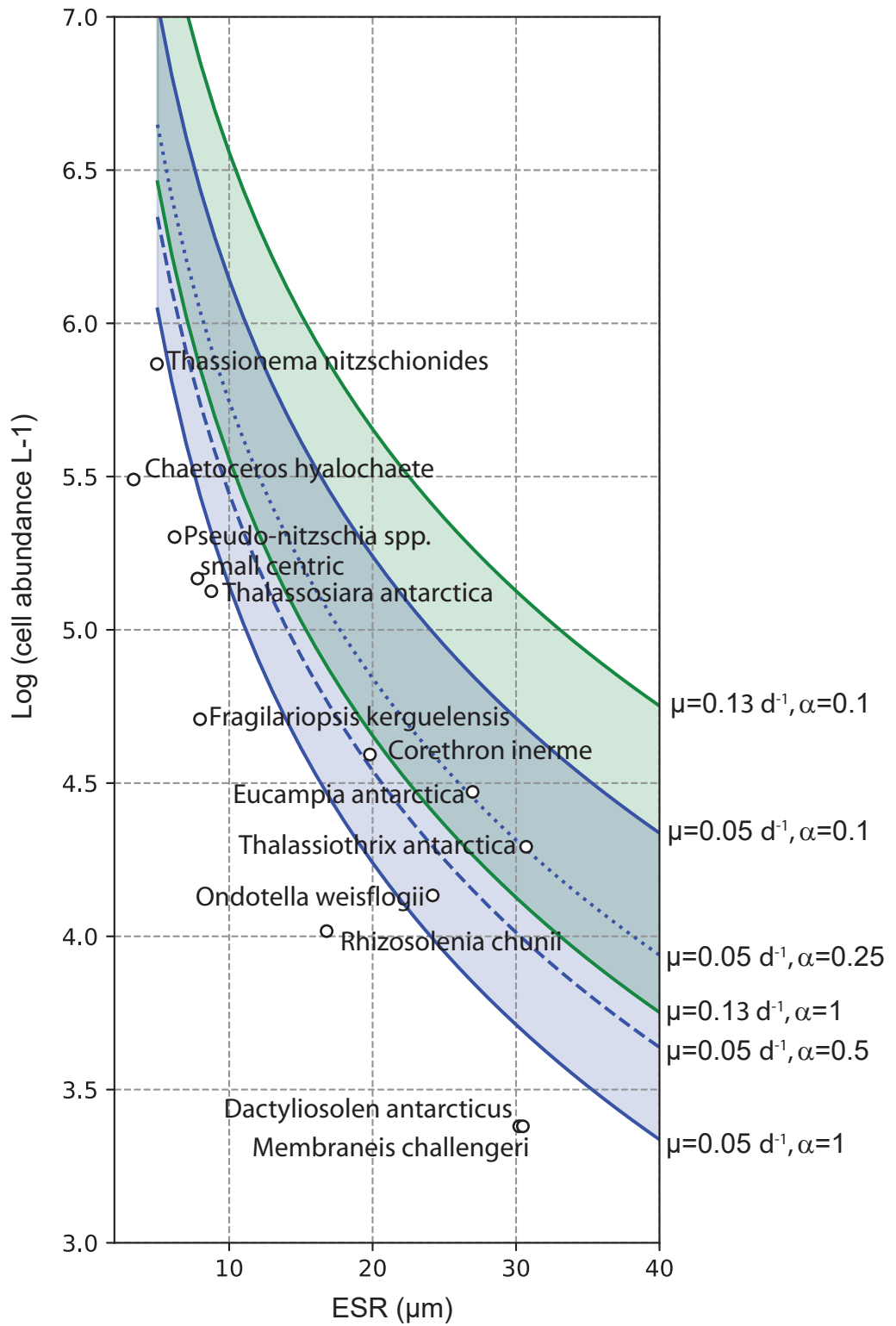


Figure 6